JACS
JOURNAL OF THE AMERICAN CHEMICAL SOCIETY
Article
pubs.acs.org/JACS

Ab Initio Structure Search and in Situ ^{7}Li NMR Studies of Discharge Products in the Li–S Battery System

Kimberly A. See,[§] Michal Leskes,[†] John M. Griffin,[†] Sylvia Britto,[†] Peter D. Matthews,[†] Alexandra Emly,[⊥] Anton Van der Ven,[∥] Dominic S. Wright,[†] Andrew J. Morris,*[,#] Clare P. Grey,*[,†,‡] and Ram Seshadri*[,§,∥]

[§]Department of Chemistry and Biochemistry and Materials Research Laboratory and [∥]Materials Department, University of California, Santa Barbara (UCSB), Santa Barbara, California 93106, United States

[†]Department of Chemistry, University of Cambridge, Lensfield Road, Cambridge CB2 1EW, United Kingdom

[⊥]Department of Materials Science and Engineering, University of Michigan, Ann Arbor, Michigan 48105, United States

[#]Theory of Condensed Matter Group, Cavendish Laboratory, University of Cambridge, J. J. Thomson Avenue, Cambridge CB3 0HE, United Kingdom

[‡]Department of Chemistry, SUNY Stony Brook, Stony Brook, New York 11794, United States

Supporting Information

ABSTRACT: The high theoretical gravimetric capacity of the Li–S battery system makes it an attractive candidate for numerous energy storage applications. In practice, cell performance is plagued by low practical capacity and poor cycling. In an effort to explore the mechanism of the discharge with the goal of better understanding performance, we examine the Li–S phase diagram using computational techniques and complement this with an in situ ^{7}Li NMR study of the cell during discharge. Both the computational and experimental studies are consistent with the suggestion that the only solid product formed in the cell is Li_2S, formed soon after cell discharge is initiated. In situ NMR spectroscopy also allows the direct observation of soluble Li^+-species during cell discharge; species that are known to be highly detrimental to capacity retention. We suggest that during the first discharge plateau, S is reduced to soluble polysulfide species concurrently with the formation of a solid component (Li_2S) which forms near the beginning of the first plateau, in the cell configuration studied here. The NMR data suggest that the second plateau is defined by the reduction of the residual soluble species to solid product (Li_2S). A ternary diagram is presented to rationalize the phases observed with NMR during the discharge pathway and provide thermodynamic underpinnings for the shape of the discharge profile as a function of cell composition.

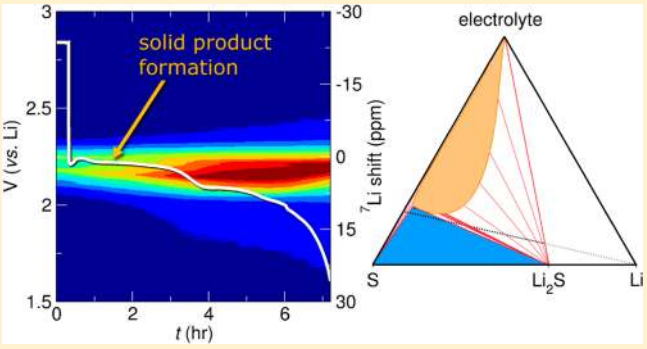

1. INTRODUCTION

The possibility of high gravimetric capacity of the Li–S battery system (1675 mA h g^{-1} assuming full S^0 reduction to S^{2-}) makes it an attractive candidate for energy storage applications where battery weight is of the highest importance, including electric vehicle and mobile electronics applications. The comparatively added benefit of the Li–S system is the low cost and greater availability of the electrode materials. The commercial success of this system is limited due to poor cell performance. In practice, the cell is plagued by low capacity and poor cycling for a variety of reasons including the low ionic and electronic conductivity of sulfur[1] and the formation of soluble intermediates.[2] It is crucial for the success of this technology that the mechanism of the discharge and the origin of these issues are understood, in order to design better materials and cell configurations.

The Li–S discharge somewhat unusually exhibits two plateaus,[3] for which several proposed mechanisms have been put forward. Direct evidence for these mechanisms is difficult to obtain due to multistep reactions that are further complicated by the formation of a variety of transient species. To summarize what is widely accepted, the first discharge plateau is believed to result in the formation of relatively long chain polysulfides, often suggested to be Li_2S_8 and Li_2S_6, while the second plateau results in further reduction to shorter chain polysulfides often denoted as Li_2S_4, Li_2S_2, and finally, Li_2S.[4] It is thought that most of these intermediate species are formed as the result of a cascading reduction starting from solid S to produce dissolved species in the electrolyte with the solubility decreasing as the chain length of S decreases until finally, two solid products are nominally formed: Li_2S_2 and Li_2S.[4]

Various ex situ techniques have been used to probe this proposed mechanism and have often resulted in contradictory

Received: August 31, 2014
Published: November 10, 2014

   dx.doi.org/10.1021/ja508982p | J. Am. Chem. Soc. 2014, 136, 16368–16377

conclusions regarding the nature of intermediate species and the final discharge product. The formation of amorphous solids and dissolved salts limits the use of commonly employed battery characterization techniques such as X-ray diffraction (XRD). Identifying intermediate species is often difficult as species in solution are dynamic and constantly undergoing disproportionation reactions,[5−7] additionally creating challenges in the interpretation of ex situ measurements. Ex situ measurements of the electrodes themselves can also be flawed as electrodes after cell disassembly can be contaminated with intermediates that would otherwise be in solution.

The apparently contradictory results of many ex situ characterization techniques highlight the need for robust in situ characterization. A handful of in situ techniques have been explored to reveal details regarding the mechanism of the Li−S discharge. Nelson et al. determined with in situ XRD and transmission X-ray microscopy that crystalline Li_2S is not formed at the end of discharge and most of the intermediate polysulfides are retained inside the cathode matrix.[8] Lowe et al. also used in situ XRD and coupled it with absorption spectroscopy to show that a limited number of polysulfide intermediates are involved in the discharge.[9] Patel et al. were able to detect soluble polysulfides in the separator using in situ UV−vis spectroscopy.[10] The peak in the UV−vis, corresponding to the polysulfides in the separator, gradually shifts to shorter wavelengths during discharge indicating the shift from long to short chains of S, consistent with the previously suggested mechanisms.[10] Cuisinier et al. presented in situ X-ray absorption spectroscopy (XANES) data that provided more details on the different pathways.[11] The XANES suggests the first plateau is governed by the reduction of S_8 to S_8^{2-} followed by disproportionation of S_8^{2-} to S_6^{2-} and S_8.[11] The voltage then drops to the second plateau due to a supersaturation of polysulfides in the electrolyte, which has been proposed to prevent further S_8 reduction.[11] XANES detects Li_2S formation near the middle of the second plateau, and this formation increases at the end of discharge.[11] No Li_2S_2 formation is detected.[11]

The strengths of these different techniques allow for unique information to be gained from each. Here, we focus on understanding the nature of intermediate species formed, whether in the solid state or in solution, to determine the possible causes of poor performance in the Li−S cell. We employ density functional theory (DFT) methods to probe the phase space between Li and S_8 and determine the possible thermodynamically favored solid-state phases formed during operation of the Li−S cell and apply this insight to the interpretation of in situ ^{7}Li nuclear magnetic resonance (NMR) measurements. In situ ^{7}Li NMR has proven to be a valuable tool to study dendrite formation on Li metal anodes,[12] structural changes in Si electrodes during cycling,[13] and Li insertion into graphite[14] and disordered carbons.[15] To probe the nature of the possible solid products, ab initio random structure searching (AIRSS) is carried out for various Li_xS_{1-x} compounds. AIRSS has been successful in predicting the ground-state structures of high-pressure phases of matter.[16] More recently it has also been applied to the Li−P[17] systems along with defects in semiconductors[18,19] and Li-ion batteries.[20,21] We complement the AIRSS algorithm with direct enumeration of vacancy-lithium disorder over sites of solid S and Li_2S. We find from both approaches that the only expected crystalline phase is Li_2S, which we corroborate experimentally by X-ray diffraction (XRD). ^{7}Li NMR has been used previously to probe the products of the Li−S discharge and charge ex situ proving to be a sensitive probe to detect both dissolved and solid Li^+ species.[22] With in situ NMR, the increase in dissolved Li^+ and Li^+-containing solid is observed during the discharge. The formation of solubilized Li^+ increases steadily during the discharge concurrent with the formation of a Li^+-containing solid component, most likely Li_2S, which forms near the beginning of the first plateau, much earlier in the discharge than previously suggested.

2. COMPUTATIONAL DETAILS

Method 1. DFT methods were used to determine possible structures and their quadrupolar coupling constants, C_Q, in the Li_xS_{1-x} phase space. Possible structures between Li and S were probed using AIRSS for a number of stoichiometries Li_xS_y where $1 > x > 8$ and $1 > y > 8$. High-throughput relaxations were also performed using the crystal structures of the known phases of Li−O, Li−S, Li−Se, Li−Te, Na−O, Na−S, Na−Se, and Na−Te. For each structure, the anions were replaced with S and the cations with Li. The structures were relaxed using forces calculated with DFT. Calculations were performed using the plane wave CASTEP DFT code,[23] and the Perdew−Burke−Ernzerhof (PBE) exchange−correlation functional was used with Vanderbilt ultrasoft pseudopotentials.[24] A basis set containing plane waves with energies of up to 500 eV and a Monkhorst−Pack (MP) grid corresponding to a Brillouin zone (BZ) sampling grid finer than $2\pi \times 0.05$ Å^{-1} was used. Electric field gradients were calculated to obtain the quadrupolar coupling constant, C_Q, for crystallographically inequivalent Li and S sites in each structure. These parameters were then averaged for each atomic species within each structure to aid the visualization of trends for the large number of structures involved.[25] Chemical shielding calculations were performed using a larger basis set, 750 eV, and finer BZ sampling $2\pi \times 0.03$ Å^{-1}.[26,27]

Method 2. Additional formation energies of structures at low x (Li_xS_{1-x}) were calculated with first-principles using DFT with PBE exchange−correlation[24] as implemented in the Vienna Ab Initio Simulation Package (VASP)[28] to supplement the AIRSS results. Projector augmented wave[29,30] pseudopotentials were used. All three electrons of Li were treated as valence electrons, and an energy cutoff of 400 eV was used. Polysulfide structures with low-Li compositions were created by introducing one Li atom into 68 candidate interstitial sites found using a Voronoi diagram of orthorhombic sulfur, which is comprised of S_8 rings. The Wyckhoff positions of the two lowest energy structures from the Li_1S_{32} configurations were found, and then additional new structures were enumerated using the CASM code.[31,32] Calculations were performed for 62 and 27 structures having compositions Li_8S_{32} and Li_2S_{32}, respectively. Higher Li-content compositions (above $x = 1/3$) were calculated by placing Li^+ into the interstitial sites of face centered cubic (fcc) and hexagonal close packed (hcp) S_8. The formation energy of Li_2S was also calculated using the antifluorite crystal structure to check agreement with Method 1.

3. EXPERIMENTAL DETAILS

Solutions for ex situ NMR experiments on varying concentrations of polysulfides in the electrolyte solvent were prepared in an Ar glovebox. A stock solution of 1 M lithium bis(trifluoromethane) sulfonamide (LiTFSI) in 1,3-dioxolane (DOL)/dimethoxyethane (DME) (1:1, v/v) electrolyte was first prepared and used as the dilution solution for the remainder of the series. A solution of 0.25 M nominal "Li_2S_6" (0.50 M Li and 1.5 M S) was prepared by mixing in the appropriate quantities of Li_2S and S_8 into the electrolyte solution and stirring at 80 °C for 2 days. Similarly, a 0.25 M solution of nominal "Li_2S_8" (0.5 M Li and 2 M S) was prepared. To obtain a series of concentrations, the concentrated 0.25 M solutions were diluted with the stock electrolyte solution to achieve the desired concentrations. Solution ^{7}Li NMR was performed on a Bruker AVANCE500 MHz spectrometer in screw-cap NMR tubes. Sealed capillaries filled with chloroform-*d* were

dx.doi.org/10.1021/ja508982p | J. Am. Chem. Soc. 2014, 136, 16368−16377

placed in the NMR tube along with the sample to achieve a lock without sacrificing the integrity of the polysulfide solutions.

Bag cells were prepared for in situ NMR experiments. The cathode was prepared by hand grinding sulfur (0.073 g, Sigma-Aldrich), Super P (0.031 g, TIMCAL), and carbon nanofibers (0.031 g, Sigma-Aldrich). Polytetrafluoroethylene (0.015 g, Sigma-Aldrich) was then added and ground until a shiny film was achieved. The cathode is composed of S/Super P/carbon nanofiber/PTFE at a weight ratio of 50:20:20:10, respectively. The 1 M LiTFSI in DOL/DME (1:1, v/v) electrolyte was prepared by first drying the LiTFSI salt (3 M Fluorad) under <3 mbar vacuum at 150 °C overnight. Dry DME was acquired from a solvent still, and the DOL (Sigma-Aldrich) was dried with molecular sieves prior to use. The bag cells were prepared in an Ar glovebox using a Li metal anode and a glass fiber filter separator (Whatman, GF/D). The free-standing cathode was pressed into a carbon-coated Al mesh, and the Li metal anode was pressed into a Cu mesh. The cells were prepared about 45 min prior to the start of NMR measurements.

In situ NMR measurements were performed on a 7T OXFORD instruments magnet, at a ^{7}Li Larmor frequency of 117.2 MHz, with a Tecmag Lap NMR console. A Bruker single channel static probe was used with a 6 mm homemade coil. Spectra were acquired with a single pulse excitation at an RF nutation frequency of 109 kHz, a $\pi/2$ pulse of 2.3 μs and a relaxation delay of 10 s. Chemical shifts were referenced with respect to a 1 M LiCl aqueous solution set at 0 ppm. 1D spectra were acquired continuously by adding 88 scans for signal averaging (1D experiment time of 14 min 40 s). The spectra were fit with the DMFit program developed by Massiot et al.[33] The errors shown are the errors relating to each parameter of the fit, as reported by DMFit. A Biologic VSP (Ultimate Electrochemical Workstation) was used for discharging the cell in situ at a rate of C/20 from open circuit voltage to 1.5 V.

4. RESULTS AND DISCUSSION

DFT was used to calculate the formation energies of several possible intermediate species in several stoichiometries of Li_xS_{1-x}. The Li_2S fluorite phase creates the bottom of a deep convex hull between the Li and S end members (Figure 1b). All predicted intermediate phases between Li and S_8 lie well above the convex hull indicating that their formation is thermodynamically unfavorable. This holds true for Li_2S_2, which is commonly suggested as a solid product during the discharge process prior to Li_2S formation. The results of the calculated phase diagram agree well with the experimental partial phase diagram.[34] The lowest energy relaxed phase for the Li_2S_2 stoichiometry is 66 meV (at 0 K) above the hull suggesting that this phase is very unlikely to form from a thermodynamic perspective. From the results of the convex hull calculations, the expected discharge curve of an all solid-state Li–S system would consist of a single plateau at 1.99 V (vs Li) due to a direct conversion to Li_2S (Figure 1c). Undoubtedly, conventional Li–S batteries with organic electrolyte are not solid-state systems as the electrolyte is actively employed during the discharge as evidenced by the formation of solubilized intermediates. Two plateaus are observed in the discharge profile rather than the single plateau expected for an all solid-state system. In order to identify the true mechanism, a much more complex phase diagram is required to correctly describe the system, which includes the activity of the solvent. However, the suggested discharge profile for a pure solid-state cathode (Figure 1c) could explain the mechanisms observed for Li–S batteries that utilize ceramic and even polymer electrolytes.[35,36]

The absence of solid-state phases other than Li_2S was verified experimentally by attempting to synthesize the intermediate stoichiometries with several preparation conditions. Refluxing *n*-butyl lithium with sulfur in toluene, heating Li_2S and sulfur

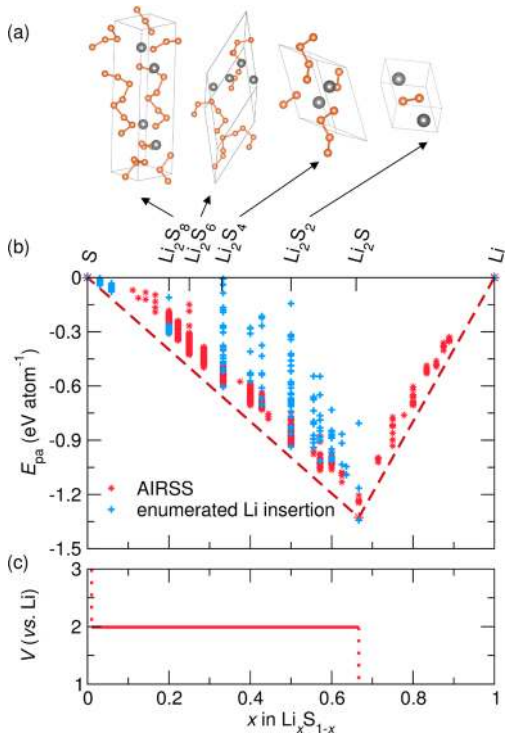

Figure 1. (a) The lowest energy solid-state structures in the Li_xS_{1-x} phase diagram, identified for Li_2S_8, Li_2S_6, Li_2S_4, and Li_2S_2, i.e., with stoichiometry Li_2S_y, all contain S chains of length y. These are all metastable phases, with respect to S and Li_2S. (b) Formation energies of several possible stoichiometries of Li with S normalized per atom (pa) using two different methods: ab initio structure searching, AIRSS (Method 1) and structures obtained by Li^+ insertion into enumerated vacancy sites in fcc or hcp S_8 (Method 2). All intermediate structures lie above the convex hull indicated by the dashed line indicating that Li_2S is the only favored solid-state phase in this system. (c) The convex hull suggests that the discharge of an all solid-state Li–S battery would exhibit a single plateau at 2 V (vs Li) corresponding to one two-phase region and direct conversion to Li_2S.

under Ar in a Parr pressure vessel, and solvothermal syntheses of *n*-butyl lithium with sulfur in toluene in a Parr pressure vessel all failed to produce new phases. The only materials identifiable by XRD were Li_2S and S_8. Higher targeted S:Li ratios result in the formation of more crystalline Li_2S suggesting that excess S drives Li_2S precipitation. The XRD of the prepared compounds along with their solid-state ^{7}Li NMR can be found in the Supporting Information. Similarly, Cuisinier et al. observe only Li_2S and S_8 phases in XRD when attempting to prepare Li_xS_y materials using yet another method: reducing S_8 with $LiEt_3BH$ in tetrahydrofuran.[11] Additionally, there is very little or no experimental evidence for solid Li_2S_2 formation in the literature. Our inability to isolate Li_2S_2 experimentally coupled with the results from the DFT calculations strongly suggests that Li_2S_2 does not form as a solid phase during the discharge. This agrees well with the recent in situ XANES studies by Cuisineier et al.[11]

Despite the very low probability that intermediate solid lithium polysulfide structures will form, it is interesting to explore the structural trends in phases closest to the hull (Figure 1). The quadrupolar coupling constants, C_Q, of the ^{7}Li nuclei in the lowest energy structures in a number of stoichiometries, were calculated and plotted (Figure 2). The magnitude of the C_Q is dictated by the symmetry and distortion of the local bonding environment and changes in these values

dx.doi.org/10.1021/ja508982p | J. Am. Chem. Soc. 2014, 136, 16368–16377

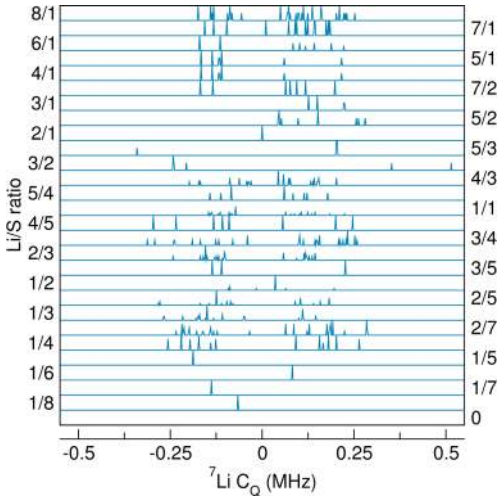

Figure 2. Calculated quadrupolar coupling constants, C_Q, for the ^{7}Li nuclei of the low-energy compounds in the series Li_xS_{1-x}. The distributions of C_Q values for each Li atom in 28 stoichiometries found by AIRSS are shown as histogram plots with the height of the line indicating the number of atoms exhibiting that C_Q.

are one measure of structural trends. All the calculated ^{7}Li C_Q values are nonzero throughout the series save for Li_2S (Figure 2), which exhibits a C_Q value of 0 MHz owing to the tetrahedral bonding environment of Li in the fluorite structure.

The ^{33}S nucleus exhibits an interesting trend as the stoichiometry changes (Figure S1). As expected, the magnitude of the C_Q is much higher for ^{33}S than for ^{7}Li. The dependence of the C_Q on the bonding environment allows for interesting structural information to be obtained from the C_Q values. An extended discussion of these structural trends can be found in the Figure S1 caption. Additionally, the ^{33}S chemical shift could also be a useful metric to identify solid intermediates since the distribution of calculated ^{33}S chemical shifts move to higher frequencies as the S-content increases (see Figure S2).

Although the solid-state phases of the intermediate stoichiometries are not expected to form (Figure 1b), we expect solubilized S_x^n species to exhibit similar chain-like bonding environments and thus similar ^{33}S chemical shifts and C_Q values. A recent DFT study by Pascal et al. shows that the structures of dissolved lithium polysulfides, as predicted by first-principles calculations, exhibit the same structural trends that AIRSS predicts for the low-energy solid-state structures, i.e., dissolved Li_2S_y exhibits a chain of S atoms with two terminal S atoms and $(2 - y)$ S atoms within the chain.[37] Therefore, in principle, ^{33}S NMR could be useful to determine solubilized species forming during the Li–S discharge noting that experimentally we are only sensitive to the C_Q parameters indirectly via, for example, relaxation phenomena. However, the low natural abundance (0.76%), large quadrupole moment, and low receptivity of ^{33}S make it a very difficult nucleus to probe with both solid and liquid NMR. Successful solution ^{33}S NMR has only been achieved on highly symmetrical molecules such as sulphones[38,39] and organic compounds when using high rf power levels, high magnetic field, and extensive signal averaging.[40] We suggest that measuring ^{33}S NMR would be useful to probe the Li–S system if spectra with sufficient signal-to-noise could be achieved. However, ^{33}S NMR would be difficult in an in situ setup and was therefore not considered for this study.

Instead, we utilize ^{7}Li NMR to explore the nature of intermediates and products formed during Li–S discharge. Since the solution products are key reaction intermediates during discharge, we first explore the sensitivity of ^{7}Li NMR to changes in Li^+ and S_x^{2-} concentrations. During cell operation, an increase in dissolved Li^+ concentration must coincide with an increase in S_x^{2-} concentration. To simulate this effect, Li^+ and S_x^{2-} are titrated into the electrolyte solution at a ratio of 1:3 and 1:4 (Figure 3). The titration experiments indicate that the resonance frequency varies significantly with the ion concentration (Li^+ and S_x^{2-}) but only mildly with the length of the S chain.

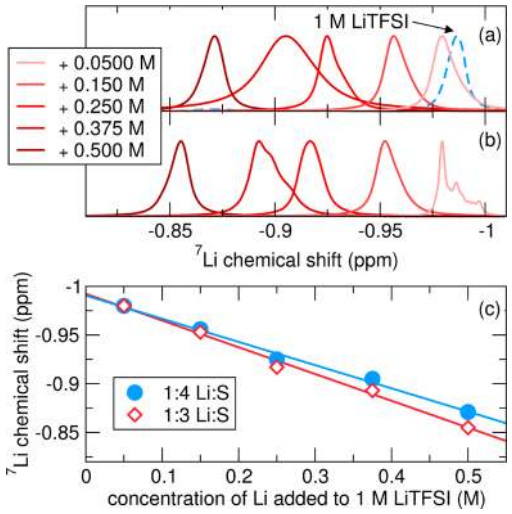

Figure 3. Solution NMR spectra of varying concentrations of Li^+ + S_x^{2-} in the electrolyte, 1 M LiTFSI in DOL/DME. In (a) a 1:4 Li:S starting ratio was employed, while in (b) the ratio was 1:3 Li:S. (c) The chemical shift displays a linear dependence on the concentration in each case. A lower Li:S ratio causes a smaller signal shift to higher frequencies.

Therefore, we can expect the ^{7}Li signal to shift to more positive frequencies with increasing concentration of the polysulfide in the electrolyte with a slight increase in shift as the S chain lengths are reduced (and the S ions are further reduced). This agrees well with the ^{7}Li NMR spectra reported by Patel et al. that also exhibit shifts to lower frequencies as the Li:S ratio decreases.[22] This shift is probably due to the increased probability that Li^+ ions are found in a S-rich solvation sphere causing a deshielding of the Li^+ but may also be due to changes in the Li^+ coordination number. There is no trend in the line width as the concentration of S increases suggesting a negligible change in viscosity up to 2.0 M S. The shift of the ^{7}Li resonance to higher frequencies due to an increase in ion concentration can be used to help interpret the in situ ^{7}Li NMR spectra during the discharge of a Li–S bag cell.

Because the chemical shift range of ^{7}Li in diamagnetic compounds is very small, it is difficult to identify intermediates directly. Instead, the NMR spectra are used to track the evolution of solubilized vs solid products as the cell discharges, since the solid components generally result in broader signals due to the presence of anisotropic interactions (such as homonuclear dipolar interactions and quadrupole couplings); these interactions are averaged out on the NMR time scale by fast tumbling of the soluble species, generally resulting in narrow line widths for the solution components.

dx.doi.org/10.1021/ja508982p | J. Am. Chem. Soc. 2014, 136, 16368–16377

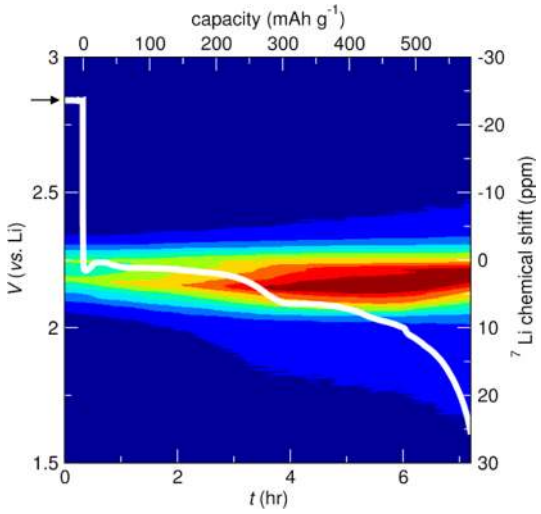

Figure 4. In situ ^{7}Li NMR signal overlaid on the electrochemical discharge curve for a Li−S bag cell discharged galvanostatically at a rate corresponding to C/20, using a 1 M LiTFSI in DOL/DME electrolyte. A spectrum is recorded every 14.6 min. The cell is held at open circuit for 15 min before discharge. The Li metal resonance at +250 ppm[12] is not shown.

Monitoring the ^{7}Li signal as the discharge progresses reveals an increase in dissolved Li^+ (sharp signals) as well as the formation of a solid component containing Li^+ (broad resonance) (Figure 4). The NMR signal is initially composed of two sharp signals corresponding to two Li^+ environments in solution (Figure 5a). There are two possible explanations for

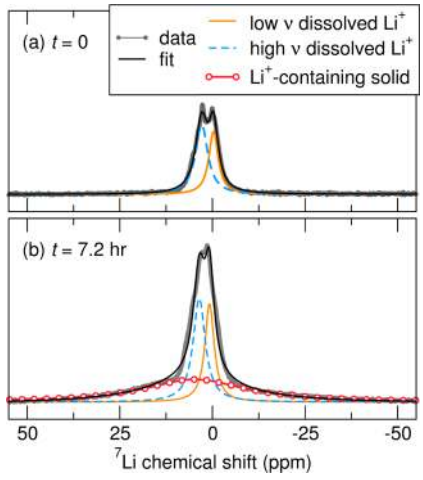

Figure 5. (a) A fit to the NMR line shape at t = 0 reveals two resolvable sharp resonances, assigned to solution species, one at higher frequencies, ν, and one at lower frequencies. (b) A third broader component, assigned to a solid phase, is clearly distinguishable at full discharge.

the origins of the two peaks. First, Li^+ ions in solution can experience different local magnetic fields in different parts of the battery (for example, within the separator, the pores of the electrode, and at the edges of the cell) due to bulk magnetic susceptibility effects caused by the different susceptibilities of the different components in the cell.[41] As shown in Figure S3, even the separator causes a noticeable susceptibility shift of 1 ppm. Second, dissolved S is present prior to discharge because of the time lag between cell fabrication and cell operation, which allows for some dissolution as evidenced by a color change of the electrolyte. This may cause a shift in the Li^+ resonance, presumably based on the ex situ experiments, to higher chemical shifts. Note that the observation of a distinct shift must similarly imply that the two Li environments are confined in different regions of the cell and cannot exchange on the time scale of the NMR experiment.

Noticeable changes in intensity and shifts of the resonances occur as the cell discharges (Figure 6). The spectrum at the end

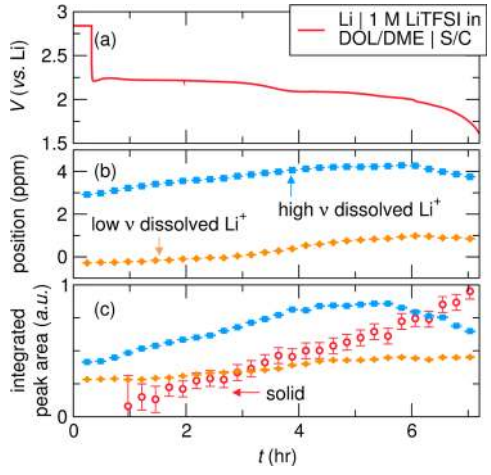

Figure 6. (a) The discharge profile of the Li−S bag cell discharged at C/20 and studied by NMR spectroscopy. The spectra were fit using the three components described in Figure 5 to extract the changes in (b) chemical shift and (c) integrated intensities as a function of discharge. The errors bars in (b) and (c) indicate the error of the fit as reported by the DMFit program.

of the discharge (Figure 5b) can be deconvoluted with three different contributions, the two sharp resonances from the dissolved Li^+ contributions and a broader resonance. The entire in situ NMR data set was therefore fit fixing the widths of the sharp resonances but allowing the line width of the broad resonance to float and good fits are obtained throughout (Figure 6b,c). The integrated area of the higher frequency, sharp Li^+ resonance increases as the cell discharges, which we ascribe to the dissolution of polysulfides (Figure 6c). We therefore assign this resonance to the Li ions in the electrolyte close to the carbon electrode, which will contain a higher concentration of polysulfides. The shift of the higher frequency resonance to even higher frequencies agrees well with the conclusion from the ex situ data that high ion concentrations cause a positive shift in the Li^+ resonance (Figure 6b). The quantity of Li^+ exhibiting a lower frequency resonance stays relatively constant as the cell discharges which suggests that the dissolution of polysulfides is limited mostly to electrolyte near the cathode structure and the migration of the polysulfides through the separator to different regions of the battery is not significant at least during the first discharge. This was also suggested previously by in situ transmission X-ray microscopy.[8]

The calculations and experimental data strongly suggest that the broad resonance is due to the solid phase, Li_2S. The chemical shift of the broad resonance is difficult to determine accurately in the spectra acquired in the initial stages of discharge due to its broad nature and low intensity. Near the end of discharge, the intensity of the broad signal is sufficient to measure the chemical shift. The resonance shifts from ∼2 to ∼4 ppm, values that are similar to those determined for Li_2S in a

dx.doi.org/10.1021/ja508982p | J. Am. Chem. Soc. 2014, 136, 16368−16377

separate magic angle spinning experiment (2.3 ppm) and by Patel et al. (2.5 ppm).[22] The initial broadness of the signal also results in larger errors associated with the fit, as shown in Figure 6c. The error reduces to about ±6% for subsequent fits, which is calculated by propagating the largest error (for fits performed on the spectra collected after 2 h of discharge) reported by DMFit for the width and amplitude, assuming the error of the integrated area is proportional to that of width × amplitude. The width of the Li^+-containing solid resonance is narrower than that measured for Li_2S ex situ (Figure S4). The line shape could be narrower because the Li_2S formed electrochemically may be disordered or contain defects, which may result in higher Li^+ mobility (resulting in reduced broadening due to ^7Li homonuclear dipolar coupling). This decreased line width is similar to that observed for the highly disordered form of Li_2S formed with high Li:S ratios during our attempts to synthesize different Li_xS_{1-x} phase (see Figure S6). It is important, however, to consider alternative Li^+-containing phases that could form during cell operation, which include solid electrolyte interphase (SEI) components forming at the anode and other lithium sulfides. Li^+ in a noncubic environment is associated with nonzero values of C_Q, the quadrupolar interaction giving rise to distinctive satellite transitions from which the C_Q values can be extracted. We have used this methodology to analyze the decomposition products formed in a Li–air battery.[42] The Li^+ environments in crystalline Li_2S are cubic, and no satellite transitions are expected (Figure 2). In contrast, all other stoichiometries of Li_xS_{1-x} (Figure 2), common SEI components[43] such as lithium alkoxides, known to form in ethereal solvents,[44] and lithium hydroxide,[45] have nonzero C_Q values and, as shown for the ^7Li NMR spectrum of lithium methoxide in Figure S5, should have clearly resolved satellite transitions. Careful examination of a larger chemical shift range reveals no evidence for any significant satellite transitions even when the spectra are added together to improve the signal-to-noise ratio.

Further evidence that the Li^+-containing solid is a result of electrochemical processes comes from the observed rate of formation. Because one electron is pulled from the anode to produce one Li^+ ion, the current and the rate of formation of Li^+ should be equal if the Li^+ formation is due to electrochemical processes. Indeed, the integrated area as the discharge progresses exhibits a linear trend, as would be expected for a galvanostatic discharge, and thus we suggest that the formation of the Li^+-containing solid is a result of electrochemical reactions (Figure 7). Near the beginning of discharge, the formation of the solid species is very likely due to electrochemical processes and not chemical reactions due to shorting, i.e., the deposition of Li_2S at the anode due to the reduction of polysulfide ions (i.e., the polysulfide shuttle),[46] since we observe a linear rate of formation. A positive deviation from linearity would be expected if Li^+ formation was due to Li_2S deposition on the anode due to an increase in Li^+ content that is unaccounted for by the current. Absence of a positive deviation from the linear fit is consistent with our suggestion that the diffusion of polysulfides into the bulk electrolyte is minimal.

It is important to note that this study considers only the first discharge and the cell is constantly polarized during the entire NMR experiment. Thus, polysulfide diffusion to the anode could occur during charging when the cell is polarized in the opposite direction. Additionally, if Li_2S formation at the anode occurs at the beginning of discharge, this process could slow

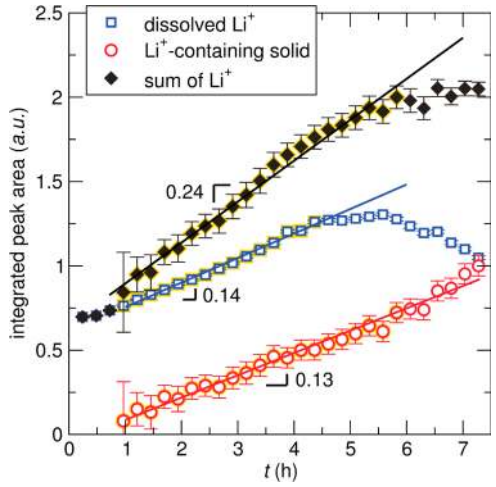

Figure 7. Integrated area of the dissolved Li^+, the Li^+-containing solid, and the sum of all Li^+ components taken from the fits of the ^7Li NMR spectra of the Li–S cell as the discharge progresses. The slope of the Li^+ formation is linear which would be expected if the Li^+ formation was due to electrochemical processes. Initially, the rates of formation of solid and dissolved products are almost the same. The linear trendlines were fit using the highlighted linear regions. A fit to the plot of the sum of Li^+ components gives a slope of 0.27 au hr^{-1} if the fit is constrained to the same region used for the individual components.

down near the end of discharge due to passivation of the anode by Li_2S. This phenomenon could potentially cause a negative deviation from linearity near the end of discharge due to an artificially high formation of Li^+ near the beginning, however, it is unlikely that the rate of formation of Li^+ due to shorting would be linear and agree so well with the rate of formation of the dissolved Li^+ as we observe here. Therefore, we believe this explanation to be unlikely. A more in depth study to determine the quantity of Li_2S formation at the anode (for example via magnetic resonance imaging)[12] needs to be done in future studies using 2D NMR experiments that enable the deconvolution of Li^+-containing solid formation at the cathode vs the anode. Based on the data presented here, however, we suggest that the solid formation primarily occurs at the cathode due to the strong linear character of the rate of formation.

The negative deviation from linearity near the end of the discharge is likely due to an underestimation of the Li^+ phase fraction in the solid component due to the incomplete relaxation of Li^+ to their equilibrium polarization within the 10 s relaxation delay used in this experiment. Initially, the longitudinal relaxation time (T_1) is expected to be relatively short (few seconds) due to the close proximity between the Li_2S forming and the carbon in the cathode. In our prior work on conversion electrode materials, the T_1 of the solid component has been observed to depend on the thickness of the solid layer formed and distance from the conductive carbon in the electrode, which is a good source for T_1 relaxation. This spatial dependence has, for example, been seen in the CuF_2[47] and RuO_2[48] conversion systems. As the solid layer becomes thicker, fewer Li^+ ions are in contact with the carbon, and their T_1 relaxation is expected to increase until it reaches the value of bulk Li_2S (the T_1 of crystalline Li_2S is of the order of 10 s). If the Li^+-containing solid formed electrochemically exhibits relaxation times comparable to that of the bulk Li_2S measured ex situ, the largest possible error in measured intensity would be an underestimation of the signal by 40%, as estimated using

dx.doi.org/10.1021/ja508982p | J. Am. Chem. Soc. 2014, 136, 16368–16377

the relationship between T_1, signal intensity, and relaxation delay described previously.[49]

Strikingly, the Li^+-containing solid begins to form near the beginning of the first plateau for our cell setup (Figure 6c). This is significantly earlier in the discharge than previously suggested by many others. In situ XRD studies, for example, report conflicting results regarding the point at which Li_2S crystallizes, but all reports are either after the first plateau[9,50] or not at all.[8] Reflections in XRD are only visible if crystallites are large enough which limits its sensitivity. NMR techniques, on the other hand, are able to detect very small quantities of solid regardless of crystallinity and particle size. A previous ex situ NMR study also shows evidence that a solid phase is present in an electrode extracted before the onset of the last plateau.[37] With in situ NMR, we are able to observe the formation of the Li^+-containing solid concurrently with the dissolved Li^+ species and at nearly identical rates suggesting that the Li_2S is forming without significant reduction of the S_x^{2-} in solution initially (Figure 7). An alternative route for solid product formation could be as a result of disproportionation reactions of dissolved polysulfides, however, the similar rates of formation of the solid and dissolved products would require the disproportionation reaction to occur at the same rate as the formation of the dissolved polysulfides (since the rate of formation of the solid would essentially reflect the rate of the disproportionation reaction). This scenario is unlikely as the rate of formation of a solid species as a product of disproportionation likely depends on many other parameters (such as the local concentration of the polysulfide precursor, etc.), while the rate of formation of the dissolved Li^+ only depends on the current applied. Additionally, a careful analytical study by Barchasz et al. on the disproportionation reactions occurring in the Li–S cell does not suggest the formation of solid product as a result of disproportionation.[7]

At the second plateau, the quantity of Li^+ in high S concentration environments begins to decrease resulting in an increase in Li^+-containing solid formation suggesting that solid formation during the second plateau is due to S_x^{2-} reduction from solution. It is also important to note that after full discharge, a significant quantity of Li^+ in a high S concentration environment remains indicating that not all the S_x^{2-} is reduced to S^{2-}. This is evidence that the low capacity is due not only to lack of electronic contact to insulating S in the cathode but also to insufficient reduction of S_x^{2-} that is formed along the discharge path. The endothermic interaction between the dissolved, polar polysulfides, and the hydrophobic carbon surface[51] along with diffusion limitations likely prevents efficient reduction.

We propose a ternary diagram that facilitates the visualization of the Li–S discharge pathway and explains the formation of the observed phases by in situ NMR (Figure 8). The electrolyte in general contains several species but in the context of a Li–S electrochemical cell can be treated as a single component. The electrolyte forms one corner of this diagram. We note that "electrolyte" could be replaced with "electrolyte solvent" as the electrolyte salt is relatively inert with respect to the performance and mechanisms of the cell discharge.[52] The diagram exhibits a prominent single-phase region corresponding to Li^+ and polysulfide species in solution. This phase must exist because Li^+ + polysulfide solutions can be prepared easily. Point F represents the solubility of solid S in the electrolyte solvent, which should be somewhat low for ethereal solvents.[53] The single phase region then dips strongly into the ternary in order

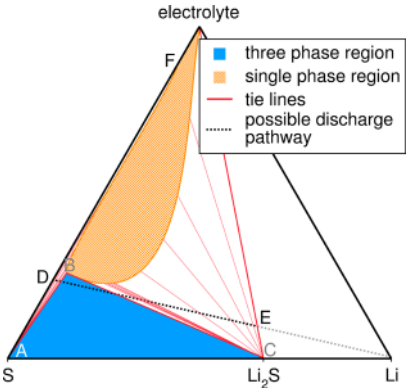

Figure 8. Proposed ternary diagram describing the pathway of the Li–S discharge. The system can only be explained using a ternary phase diagram as the electrolyte is actively involved in the discharge pathway. The approximate discharge profile would exhibit a plateau when passing through the three-phase region, a voltage drop upon exiting the three-phase region, and another plateau when passing through the two-phase regions thereafter. This would result in two plateaus, as seen in experiment.

to represent the higher solubility of long chain polysulfides (high S:Li ratio) and lower solubility of short chain polysulfides, which will be true for any low dielectric constant electrolyte solvent like ethereal solvents.[2] The bottom line of the phase diagram is the Li–S binary axis and only one solid phase exists on this line, which, as discussed above, is Li_2S according to DFT calculations (Figure 1b) and experiments. The two-phase coexistence between S and Li_2S along the binary Li–S axis will expand into a ternary composition space as a three-phase region. We propose that this three-phase region consists of S (point A), Li^+, and polysulfides dissolved in the electrolyte solvent (point B) and Li_2S (point C) as schematically illustrated by the blue triangle in Figure 8. The phase diagram also shows a large two-phase region between solid Li_2S and the electrolyte solvent. The tie lines (thin red lines) in the two-phase region represent compositions of constant chemical potentials. The particular electrolyte chemistry determines the solubility of short chain polysulfides and therefore also the size and shape of the electrolyte single-phase region in Figure 8. The lower solubility of sulfur in the electrolyte in comparison to the polysulfides is represented by point F along the S–electrolyte binary.

Based on this ternary diagram, it is possible to rationalize the sequence and compositions of the phases observed with NMR. Before discharge of the cell, the initial composition at the cathode–electrolyte interface resides on the binary S–electrolyte axis, illustrated as point D in Figure 8. For high S/electrolyte ratios at the cathode, the initial composition will lie close to pure S. Assuming local equilibrium, the composition at the cathode–electrolyte interface will follow a line to first order connecting the initial composition and the pure Li corner upon discharge. A proposed discharge pathway is shown as the dashed black line from point D to E. This line quickly passes through the three-phase region, at which point solid Li_2S will form and coexist with both solid S and dissolved Li^+ and polysulfides in the electrolyte, the latter having a fixed Li concentration. The proposed ternary diagram therefore suggests that solid Li_2S should form very early in the discharge process and is consistent with the NMR observations.

The formation of Li_2S when passing through the three-phase region will most likely occur on the preexisting S particle

dx.doi.org/10.1021/ja508982p | J. Am. Chem. Soc. 2014, 136, 16368–16377

surfaces to form a Li_2S/S core−shell morphology. This mechanism is supported by the linear increase in Li_2S formation in Figure 7 which suggests a surface reaction that does not rely on solid-state Li diffusion (which would show a characteristic parabolic time evolution). The cathode−electrolyte interface then exits the three-phase region, indicating electrochemical passivation of S probably due to Li_2S deposition, and proceeds through the two-phase region, where Li_2S formation continues, not by reducing solid S but rather by precipitating the polysulfides from the electrolyte. The reaction comes to an end once the local composition of the electrolyte−Li_2S mixture reaches the tie line connecting the Li_2S and the pure electrolyte having no dissolved polysulfides.

The schematic ternary diagram of Figure 8 also provides insight about the shape of the voltage profile. The voltage is related to the difference in chemical potentials between the cathode and the anode. In a ternary composition space, the voltage will exhibit a plateau when passing through a three-phase region or when the variation in composition is parallel to a tie line in a two-phase region. Otherwise, the voltage profile is sloping with the density of tie lines defining the grade of the slope.[54] The first plateau in Figure 6a is consistent with the proposed three-phase region in Figure 8. The initial dip in the voltage immediately before the plateau can be attributed to the polarization required to overcome a nucleation barrier to form solid Li_2S. The length of the plateau does not necessarily correspond to the length of the discharge pathway in the three-phase region (see Figure S9 for more detail). After the plateau, there is a drop in voltage indicating a passage through a set of dense tie lines between Li_2S and a very stable dissolved polysulfide. An exceptionally stable dissolved polysulfide would result in a deep well in the ternary free energy surface and allow for a large change in chemical potential without a significant change in the Li/S ratio. The voltage flattens out after the step, which could signify a three-phase region or, alternatively, as indicated by the schematic diagram of Figure 8, a two-phase region with a very low density of tie lines.

While the proposed three-phase region in Figure 8 is consistent with DFT predictions, the failure to synthesize intermediate solid lithium polysulfides, the NMR observation of the early formation of Li_2S formation, and the plateau in the voltage profile, it is inconsistent with the observed linear increase in the Li^+ in solution (Figure 7). When passing through the three-phase region, the electrolyte composition in the vicinity of the cathode should remain constant and is defined by the apex of the three-phase triangle, point B. Instead, the NMR measurements show a steady increase in lithium polysulfide content as the discharge progresses. One possible explanation for the contradiction is that the electrochemical cell as a whole is not in equilibrium. Upon approaching the bulk electrolyte (electrolyte far from the cathode), the concentration of polysulfides in the electrolyte decreases. The gradient in polysulfide concentration across the electrolyte will generate a flux of polysulfides away from the cathode. To maintain the constant polysulfide concentration at the cathode interface while passing through the three-phase region, polysulfides need to be formed at the cathode−electrolyte interface along with the solid Li_2S, thereby increasing the overall Li^+ content in the electrolyte solution. Hence, two redox reactions occur simultaneously and, as indicated by Figure 7, with the same rate. The parallel slopes in Figure 7 for Li_2S formation and Li^+ concentration in solution suggest that both reactions have the same rate-limiting step, which is presumably the transport of Li^+ from the anode to the cathode. The subsequent decrease in the concentration of Li^+ in solution is consistent with the reduction of polysulfide solubility within the electrolyte phase as the local composition passes through the two-phase region as shown in the phase diagram of Figure 8.

Any modifications of the electrolyte chemistry will affect the solubility limits of the polysulfides as well as the size and shape of the three-phase region in which Li_2S, S, and dissolved Li^+ and polysulfides coexist. Additional factors affecting the shape of the discharge profile include the starting ratio of S to electrolyte, indicated by point D in Figure 8. Furthermore, varying the surface area of S in contact with the electrolyte will indeed shift this point. Cathodes with higher S contents (all other parameters held constant) should also exhibit higher surface areas of S in contact with the electrolyte thus shifting the beginning of the discharge pathway toward the S corner. This results in a relative shortening of the second plateau, which agrees well with previously published discharge curves that study the effect of the S/electrolyte ratio on performance.[55,56] Only recently has the amount of electrolyte in the cell been shown as an important factor governing cell performance,[55−58] and this ternary diagram provides insight into how the discharge curves may change depending on the starting point of the discharge pathway. A large shift of point D (start of discharge) toward point F could cause the discharge pathway to traverse the single-phase region initially, which would define the first plateau in this case, thereby bypassing the formation of Li_2S until the two-phase region is reached during the second plateau. If Li_2S is indeed only forming during the second plateau, then the dip in the voltage, often associated with the onset and nucleation and growth of a new phase, should be observable at the beginning of the second plateau rather than the first. This could explain why other experiments and characterization techniques do not observe Li_2S formation during the first plateau and further demonstrates the utility of the ternary diagram to visualize the effect of many variables on the discharge mechanism.

5. CONCLUSIONS

Experimental and computational studies carried out here suggest that there is little or no evidence for solid products other than Li_2S during the discharge of the Li−S cell. Li^+-containing solid formation is observed near the beginning of the first discharge plateau with in situ NMR. This is a significant finding since these solids are hard to observe with other in situ techniques such as XRD as a consequence of the small crystallites that are formed and the relatively low X-ray scattering powers of Li and S. With in situ NMR we are able to see the formation of solid product independent of the particle size and crystallinity. The formation rate of Li^+-containing solid remains steady during the entire discharge and appears to not require the reduction of polysulfides in solution. It is only during the second plateau that NMR shows evidence of reduction of solubilized S_x^{2-} to solid product. The second plateau coincides with a significant decrease in Li^+ and polysulfide concentration and an increase in Li^+-containing solid formation suggesting that at this point, Li_2S is formed by reduction of polysulfides in solution. At the end of discharge, we see evidence for a significant amount of polysulfides remaining in solution. This suggests that the low discharge capacity on the first cycle is in part due to insufficient reduction of polysulfides in solution. The utility of in situ ^{7}Li NMR therefore clearly lies in its ability to distinguish solid vs

dissolved products containing Li^+ which provides further insight into the Li−S discharge mechanism in this important electrochemical energy storage system. This new insight on the phases forming during discharge has inspired a proposed ternary diagram which is able to describe the discharge pathway of the Li−S cell and provides a visualization tool to present trends already seen in the literature. The ternary diagram enables pertinent information on the phases forming during discharge to be distilled. The diagram can potentially help inspire research to overcome the limitations of the Li−S system, allowing it to reach its full potential.

■ ASSOCIATED CONTENT

Supporting Information

Calculated ^{33}S quadrupolar coupling constants and chemical shifts for various stoichiometries in Li_xS_{1-x}, effects of the separator on the ^7Li NMR resonance, comparison of the Li_2S line width to the line width of the solid formed during discharge, static ^7Li NMR of lithium methoxide, XRD and ^7Li NMR of the various attempts at preparing Li_xS_y intermediates, and the correlation of the ternary diagram to a two phase representation as it would be presented in a voltage curve. This material is available free of charge via the Internet at http://pubs.acs.org.

■ AUTHOR INFORMATION

Corresponding Authors

ajm255@cam.ac.uk
cpg27@cam.ac.uk
seshadri@mrl.ucsb.edu

Notes

The authors declare no competing financial interest.

■ ACKNOWLEDGMENTS

The authors would like to thank Dr. Jerry Hu for assistance on solution NMR experiments and Maxwell J. Robb for helpful discussions. Fellowship support to K.A.S. from the ConvEne IGERT Program of the National Science Foundation (DGE 0801627) is gratefully acknowledged. A.J.M. acknowledges the support from the Winton Programme for the Physics of Sustainability. P.D.M. and D.S.W. thank the UK-EPSRC for financial support. This research made use of the shared experimental facilities of the Materials Research Laboratory (MRL), supported by the MRSEC Program of the NSF under award no. DMR 1121053. The MRL is a member of the NSF-funded Materials Research Facilities Network (www.mrfn.org). C.P.G. and M.L. thank the U.S. DOE Office of Vehicle Technologies (contract no. DE-AC02-05CH11231) and the EU ERC (via an Advanced Fellowship to C.P.G.) for funding.

■ REFERENCES

(1) *CRC Handbook of Chemistry and Physics*, 94th ed.; Haynes, W. M., Ed.; CRC Press: Boca Raton, FL, 2013.
(2) Rauh, R. D.; Shuker, F. S.; Marston, J. M.; Brummer, S. B. *J. Inorg. Nucl. Chem.* **1977**, *39*, 1761−1766.
(3) Yamin, H.; Peled, E. *J. Power Sources* **1983**, *9*, 281−287.
(4) Kumaresan, K.; Mikhaylik, Y.; White, R. E. *J. Electrochem. Soc.* **2008**, *155*, A576−A582.
(5) Badoz-Lambling, J.; Bonnaterre, R.; Cauquis, G.; Delamar, M.; Demange, G. *Electrochim. Acta* **1976**, *21*, 119−131.
(6) Yamin, H.; Gorenshtein, A.; Penciner, J.; Sternberg, Y.; Peled, E. *J. Electrochem. Soc.* **1988**, *135*, 1045−1048.
(7) Barchasz, C.; Molton, F.; Duboc, C.; Leprêtre, J.-C.; Patoux, S.; Alloin, F. *Anal. Chem.* **2012**, *84*, 3973−3980.
(8) Nelson, J.; Misra, S.; Yang, Y.; Jackson, A.; Liu, Y.; Wang, H.; Dai, H.; Andrews, J. C.; Cui, Y.; Toney, M. F. *J. Am. Chem. Soc.* **2012**, *134*, 6337−6343.
(9) Lowe, M. A.; Gao, J.; Abruna, H. *RSC Adv.* **2014**, *4*, 18347−18353.
(10) Patel, M. U. M.; Demir-Cakan, R.; Morcrette, M.; Tarascon, J.-M.; Gaberscek, M.; Dominko, R. *ChemSusChem* **2013**, *6*, 1177−1181.
(11) Cuisinier, M.; Cabelguen, P.-E.; Evers, S.; He, G.; Kolbeck, M.; Garsuch, A.; Bolin, T.; Balasubramanian, M.; Nazar, L. F. *J. Phys. Chem. Lett.* **2013**, *4*, 3227−3232.
(12) Bhattacharyya, R.; Key, B.; Chen, H.; Best, A. S.; Hollenkamp, A. F.; Grey, C. P. *Nat. Mater.* **2010**, *9*, 504−510.
(13) Key, B.; Bhattacharyya, R.; Morcrette, M.; Seznéc, V.; Tarascon, J.-M.; Grey, C. P. *J. Am. Chem. Soc.* **2009**, *131*, 9239−9249.
(14) Letellier, M.; Chevallier, F.; Morcrette, M. *Carbon* **2007**, *45*, 1025−1034.
(15) Chevallier, F.; Letellier, M.; Morcrette, M.; Tarascon, J.-M.; Frackowiak, E.; Rouzaud, J.-N.; Béguin, F. *Electrochem. Solid-State Lett.* **2003**, *6*, A225−A228.
(16) Pickard, C. J.; Needs, R. J. *J. Phys.: Condens. Matter* **2011**, *23*, 053201.
(17) Ivanov, A. S.; Morris, A. J.; Bozhenko, K. V.; Pickard, C. J.; Boldyrev, A. I. *Angew. Chem., Int. Ed.* **2012**, *51*, 8330−8333.
(18) Morris, A. J.; Pickard, C. J.; Needs, R. J. *Phys. Rev. B* **2008**, *78*, 184102.
(19) Morris, A. J.; Pickard, C. J.; Needs, R. J. *Phys. Rev. B* **2009**, *80*, 144112.
(20) Morris, A. J.; Needs, R. J.; Salager, E.; Grey, C. P.; Pickard, C. J. *Phys. Rev. B* **2013**, *87*, 174108.
(21) Morris, A. J.; Grey, C. P.; Needs, R. J.; Pickard, C. J. *Phys. Rev. B* **2011**, *84*, 224106.
(22) Patel, M. U. M.; Arčon, I.; Aquilanti, G.; Stievano, L.; Mali, G.; Dominko, R. *ChemPhysChem* **2014**, *15*, 894−904.
(23) Clark, S. J.; Segall, M. D.; Pickard, C. J.; Hasnip, P. J.; Probert, M. I. J.; Refson, K.; Payne, M. C. *Z. Für Krist.* **2005**, *220*, 567−570.
(24) Perdew, J. P.; Burke, K.; Ernzerhof, M. *Phys. Rev. Lett.* **1996**, *77*, 3865−3868.
(25) Profeta, M.; Mauri, F.; Pickard, C. J. *J. Am. Chem. Soc.* **2003**, *125*, 541−548.
(26) Yates, J. R.; Pickard, C. J.; Mauri, F. *Phys. Rev. B* **2007**, *76*, 024401.
(27) Pickard, C. J.; Mauri, F. *Phys. Rev. B* **2001**, *63*, 245101.
(28) Kresse, G.; Furthmüller, J. *Phys. Rev. B* **1996**, *54*, 11169−11186.
(29) Kresse, G.; Joubert, D. *Phys. Rev. B* **1999**, *59*, 1758−1775.
(30) Blöchl, P. E. *Phys. Rev. B* **1994**, *50*, 17953−17979.
(31) Puchala, B.; Van der Ven, A. *Phys. Rev. B* **2013**, *88*, 094108.
(32) Van der Ven, A.; Thomas, J. C.; Xu, Q.; Swoboda, B.; Morgan, D. *Phys. Rev. B* **2008**, *78*, 104306.
(33) Massiot, D.; Fayon, F.; Capron, M.; King, I.; Le Calvé, S.; Alonso, B.; Durand, J.-O.; Bujoli, B.; Gan, Z.; Hoatson, G. *Magn. Reson. Chem.* **2002**, *40*, 70−76.
(34) Cunningham, P. T.; Johnson, S. A.; Cairns, E. J. *J. Electrochem. Soc.* **1972**, *119*, 1448−1450.
(35) Marmorstein, D.; Yu, T. .; Striebel, K. .; McLarnon, F. .; Hou, J.; Cairns, E. . *J. Power Sources* **2000**, *89*, 219−226.
(36) Zhang, Y.; Zhao, Y.; Gosselink, D.; Chen, P. *Ionics* **2014**, 1−5.
(37) Pascal, T. A.; Wujcik, K. H.; Velasco-Velez, J.; Wu, C.; Teran, A. A.; Kapilashrami, M.; Cabana, J.; Guo, J.; Salmeron, M.; Balsara, N.; Prendergast, D. *J. Phys. Chem. Lett.* **2014**, 1547−1551.
(38) Faure, R.; Vincent, E. J.; Ruiz, J. M.; Léna, L. *Org. Magn. Reson.* **1981**, *15*, 401−403.
(39) Cassidei, L.; Fiandanese, V.; Marchese, G.; Sciacovelli, O. *Org. Magn. Reson.* **1984**, *22*, 486−487.
(40) Retcofsky, H. L.; Friedel, R. A. *J. Am. Chem. Soc.* **1972**, *94*, 6579−6584.
(41) Zhou, L.; Leskes, M.; Ilott, A. J.; Trease, N. M.; Grey, C. P. *J. Magn. Reson.* **2013**, *234*, 44−57.

(42) Leskes, M.; Drewett, N. E.; Hardwick, L. J.; Bruce, P. G.; Goward, G. R.; Grey, C. P. *Angew. Chem., Int. Ed.* **2012**, *51*, 8560−8563.
(43) Peled, E. *J. Electrochem. Soc.* **1979**, *126*, 2047−2051.
(44) Aurbach, D.; Daroux, M. L.; Faguy, P. W.; Yeager, E. *J. Electrochem. Soc.* **1988**, *135*, 1863−1871.
(45) Moore, A. J.; Leskes, M.; Ball, S.; Potter, R.; Grey, C. P. *Abstract no. 414*. In Proceedings of the Electrochemical Society Meeting, San Francisco, CA, October 27−November 1, 2013; ECS: Pennington, NJ, 2013.
(46) Mikhaylik, Y. V.; Akridge, J. R. *J. Electrochem. Soc.* **2004**, *151*, A1969−A1976.
(47) Hua, X.; Robert, R.; Du, L.-S.; Wiaderek, K. M.; Leskes, M.; Chapman, K. W.; Chupas, P. J.; Grey, C. P. *J. Phys. Chem. C* **2014**, *118*, 15169−15184.
(48) Hu, Y.-Y.; Liu, Z.; Nam, K.-W.; Borkiewicz, O. J.; Cheng, J.; Hua, X.; Dunstan, M. T.; Yu, X.; Wiaderek, K. M.; Du, L.-S.; Chapman, K. W.; Chupas, P. J.; Yang, X.-Q.; Grey, C. P. *Nat. Mater.* **2013**, *12*, 1130−1136.
(49) Leskes, M.; Moore, A. J.; Goward, G. R.; Grey, C. P. *J. Phys. Chem. C* **2013**, *117*, 26929−26939.
(50) Cañas, N. A.; Wolf, S.; Wagner, N.; Friedrich, K. A. *J. Power Sources* **2013**, *226*, 313−319.
(51) See, K. A.; Jun, Y.-S.; Gerbec, J. A.; Sprafke, J. K.; Wudl, F.; Stucky, G. D.; Seshadri, R. *ACS Appl. Mater. Interfaces* **2014**, *6*, 10908−10916.
(52) Gao, J.; Lowe, M. A.; Kiya, Y.; Abruña, H. D. *J. Phys. Chem. C* **2011**, *115*, 25132−25137.
(53) Sciamanna, S. F.; Lynn, S. *Ind. Eng. Chem. Res.* **1988**, *27*, 485−491.
(54) Yu, H.-C.; Ling, C.; Bhattacharya, J.; Thomas, J. C.; Thornton, K.; Van der Ven, A. *Energy Environ. Sci.* **2014**, *7*, 1760−1768.
(55) Zhang, S. S. *Energies* **2012**, *5*, 5190−5197.
(56) Brückner, J.; Thieme, S.; Grossmann, H. T.; Dörfler, S.; Althues, H.; Kaskel, S. *J. Power Sources* **2014**, *268*, 82−87.
(57) Zheng, J.; Lv, D.; Gu, M.; Wang, C.; Zhang, J.-G.; Liu, J.; Xiao, J. *J. Electrochem. Soc.* **2013**, *160*, A2288−A2292.
(58) Doan, T. N. L.; Gosselink, D.; Hoang, T. K. A.; Chen, P. *Phys. Chem. Chem. Phys.* **2014**, *16*, 13843.